JOURNAL OF MATERIALS SCIENCE 29 (1994) 569–583

Review
Role of oxygen diffusion in polymer ageing: kinetic and mechanical aspects

L. AUDOUIN, V. LANGLOIS, J. VERDU
Ecole Nationale Supérieure d'Arts et Métiers, 151 Boulevard de l'Hôpital, 75013 Paris, France
J. C. M. de BRUIJN
Delft University of Technology, Laboratory for Mechanical Reliability, Leeghwaterstraat 35, 2628 CB Delft, The Netherlands

For an ageing process involving the consumption of a small molecule (typically O_2 or H_2O) by reaction with the polymer, there are critical conditions of reaction rate and/or thickness above which the process becomes kinetically controlled by the diffusion of the small molecule in the polymer. Suitable lifetime prediction models must then involve the thickness distribution of reaction products. This latter can be predicted from Fick's law, modified by a term relative to the rate of consumption of the diffusing species by the chemical reaction. Some problems related to the use of this approach are examined here. It appears that, in the most frequent case, the thickness of the degraded layer is of the order of magnitude of D/k, where D is the diffusion coefficient and k the pseudo-first-order rate constant for reactant consumption. Some examples of application related to photochemical, radiochemical and thermochemical ageing are examined. It can, for instance, be shown that in photochemical or radiochemical ageing, the thickness of the oxidized layer (TOL) is proportional to the reciprocal of I^{β}, where I is the radiation intensity and β an exponent depending essentially on the radical chain mechanism. It is generally expected that in the case of thermal ageing, the TOL is a decreasing function of the temperature. Some consequences of diffusion control on accelerated and natural ageing methods are briefly examined. The consequences of the ageing-induced "skin–core" structure due to the diffusion control are examined. The main features of the observed polymer embrittlement can be explained in terms of fracture mechanics.

1. Introduction

Many important ageing processes such as oxidation, hydrolysis and ozonolysis involve a reaction of the polymer with a small environmental molecule (O_2, H_2O, O_3). It can be experimentally observed that, in these cases, at a given temperature, there is a pseudo-hyperbolic boundary in the unperturbed reaction rate (r_s) versus sample thickness coordinate system (Fig. 1).

The unperturbed reaction rate r_s can be defined as the local reaction rate in a very thin superficial layer of the exposed sample. Two domains can be distinguished:

(i) Domain I: For low values of r_s and/or sample thickness L, the kinetics is not diffusion-controlled. The low molecular weight reactant is consumed homogeneously throughout the sample. The reaction rates are homogeneously distributed within the sample thickness (Fig. 2a).

(ii) Domain II: For high values of r_s and/or L, the kinetics is diffusion-controlled. Most of the low molecular weight reactant is consumed in the superficial layers of the sample. The reaction rates are heterogeneously distributed within the sample thickness (Fig. 2b–d).

In a liquid system, convection can lead to homogenization of the reaction products. In a solid system, however, large-scale motions of the reaction products are practically forbidden, so that their spatial distribution directly reflects the spatial distribution of the reaction rates. In most of the ageing literature prior to 1988, it was implicitly or explicitly assumed that the polymer (or composite) samples behaved as a liquid system, which often carried grave consequences in the interpretation of individual experimental results and in the methodological field (determination of exposure parameters in accelerated ageing, method for lifetime prediction, etc.).

In practice, two main questions arise from experimental studies on ageing:

(i) Is it possible to predict the thickness distribution of ageing products for a given polymer sample in given exposure conditions?

(ii) How does the heterogeneity of this distribution affect the (especially mechanical) use properties?

The objective of this article is first to recall the basic principles of the studies of diffusion-controlled kinetics, secondly to report recent advances in analytical methods for the study of heterogeneous degradation,

0022–2461

and thirdly to review recent work on the consequences of this heterogeneous degradation for the mechanical behaviour.

2. Kinetic equations

Most of the authors [1–10] involved in this topic have started from Fick's second law:

$$\frac{\partial C}{\partial t} = D\frac{\partial^2 C}{\partial x^2} \quad (1)$$

where C = concentration of reactant, t = time, x = depth of penetration of reactive species and D = diffusion coefficient. When the reactant is consumed by the reaction at a rate r, this becomes

$$\frac{\partial C}{\partial t} = D\frac{\partial^2 C}{\partial x^2} - r \quad (2)$$

The local reaction rate r is a function of the local reactant concentration: $r \rightarrow r(C)$. Furthermore, it can be assumed that the system reaches to a stationary state when $\partial C/\partial t = 0$, and then

$$D\frac{\partial^2 C}{\partial x^2} - r(C) = 0 \quad (3)$$

It should be possible to determine the concentration profile $C(x)$ with this differential equation, provided that D and $r(C)$ are known.

The diffusion coefficient D can be determined from classical sorption or permeation tests [11]. In the simplest case, it is a constant (expressed in $m^2 s^{-1}$ or more frequently $cm^2 s^{-1}$) independent of depth, time or concentration C. More complex situations can be imagined, for instance:

(i) The diffusion coefficient depends on the conversion of the ageing process, i.e. of time. In this case, an initially homogeneous sample becomes heterogeneous. This is for example the case with the radiochemical ageing of low-density polyethylene (LdPE) [12]. Oxidation in the superficial layers leads to chain scission with a slight increase of the O_2 permeability, whereas cross-linking in the core zone results in a decrease of the O_2 permeability (Fig. 3).

(ii) The diffusion coefficient depends on the reactant concentration. This "anomalous" behaviour can be observed in the case where high concentrations of the reactant can induce a noticeable polymer plasticization. In these cases, short-term physical ageing processes are generally responsible for very important property changes, so that the study of chemical kinetics can be considered as purely academic.

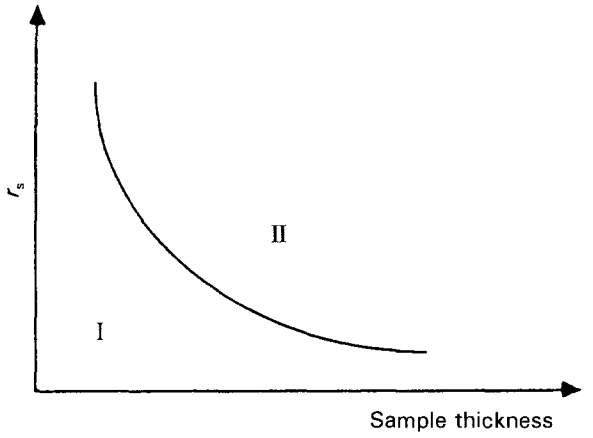

Figure 1 Ageing kinetic regimes (see text).

2.1. Variation of reaction rate

The concentration dependence of the reaction rate $r(C)$ can be determined from experiments or deduced from an analysis of the reaction mechanism.

2.1.1. Experimental determination of r(C)

This must be made on very thin samples in order to avoid any diffusion-controlled effect on the kinetics. In the most common case, where the reactant is gaseous, the simplest method is to experiment at various partial pressures of the reactant in the atmosphere. According to Henry's law, the equilibrium concentration C_s is linked to the reactant partial pressure p by the relation

$$p = SC_s \quad (4)$$

where S is a solubility coefficient expressed in Pa $m^3 mol^{-1}$. Equation 4 is generally obeyed in the cases where oxygen is the reactant. In contrast, in the case of water, deviations from Henry's law are often observed.

The dependence of the equilibrium concentration on p_{H_2O} partial pressure is often expressed by a power law:

$$\frac{C}{C_s} = H\left(\frac{p}{p_s}\right)^{\beta} \quad (5)$$

where H and β are constants, p_s is the saturated

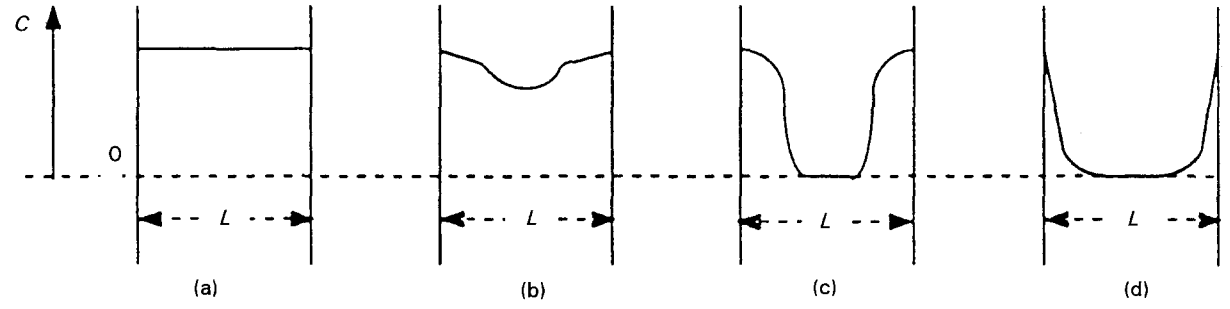

Figure 2 Thickness distribution profile of reaction products: (a) non-diffusion-controlled ageing process, (b–d) diffusion-controlled ageing process.

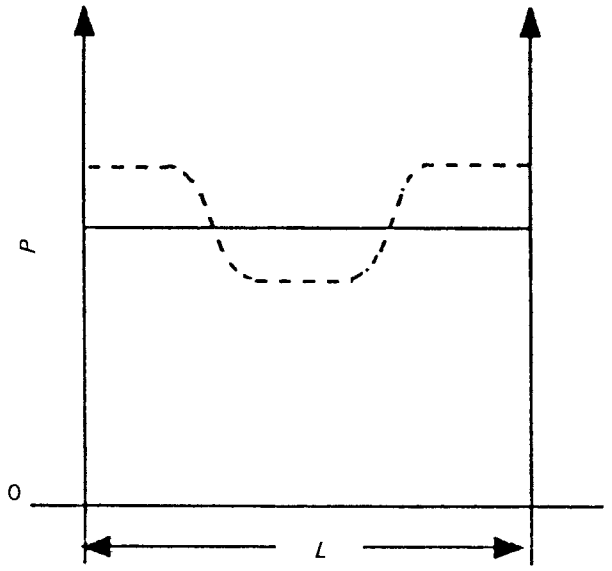

Figure 3 Thickness profile of oxygen permeability in the case of polyethylene: (—) before irradiation, (– – –) after irradiation in air or in oxygen.

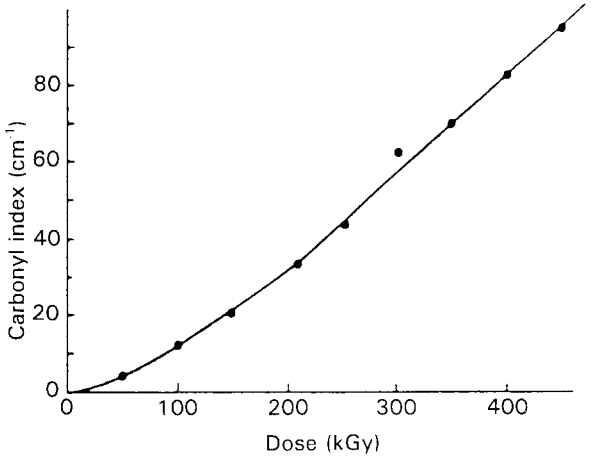

Figure 4 Carbonyl build-up during gamma-ray irradiation at 0.69 Gy s^{-1} for an LdPE film of 22 μm thickness [8].

vapour pressure and C_s the corresponding equilibrium concentration at the temperature under consideration.

An example of this approach is illustrated by Figs 4 and 5 in the case of radiochemical oxidation of polyethylene [8]. LdPE films of 22 μm thickness were exposed to gamma rays at a dose rate of 0.69 Gy s^{-1}, and their oxidation was followed by i.r. determination of carbonyl groups. The results are expressed in terms of absorbance per thickness unit (cm^{-1}), which can be converted into concentration units using

$$A = \varepsilon C$$

where $\varepsilon \simeq 0.2$ mol^{-1} cm^2, C being expressed in mol cm^{-3}. An example of a kinetic curve of carbonyl build-up is shown in Fig. 4. It can be seen that, after a short transient state, the oxidation occurs at a constant rate. This oxidation rate, expressed in cm^{-1} kGy^{-1}, is plotted in Fig. 5 against oxygen pressure.

This type of curve was observed in many oxidation experiments, including thermal ageing ones [13, 14]. It is characterized by a critical oxygen pressure p_c, i.e.

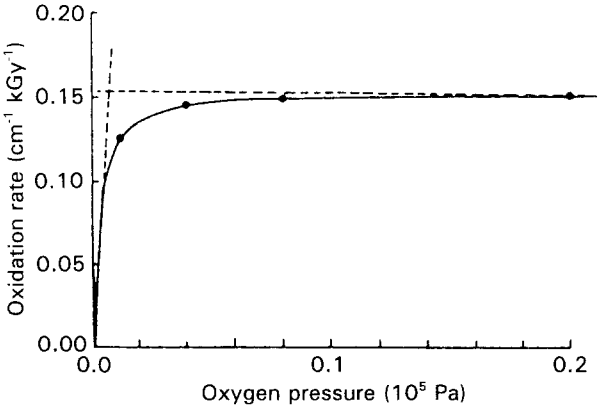

Figure 5 Rate of carbonyl build-up against oxygen pressure for an LdPE film of 22 μm thickness irradiated at 0.69 Gy s^{-1} [8].

a critical concentration C_c, above which the oxidation rate becomes practically independent of concentration. In the case under study, the critical oxygen pressure p_c was found to be lower than the atmospheric pressure: $p_c \simeq 0.01$ MPa. In other cases, however, for instance for the thermal oxidation of anhydride-cured epoxies [13, 14], a p_c value of about 0.3 MPa, i.e. about 15 times higher than the atmospheric pressure (0.02 MPa), was found.

2.1.2. Theoretical determination of $r(C)$

This can be deduced from the reaction mechanisms. Let us consider, for instance, the standard mechanistic scheme for radical chain oxidations:

Initiation:	Polymer → radicals P•	(r_i)
Propagation:	P• + O_2 → $PO_2^•$	k_2
	$PO_2^•$ + PH → PO_2H + P•	k_3
Termination:	P• + P• →	k_4
	P• + $PO_2^•$ → inactive species	k_5
	$PO_2^•$ + $PO_2^•$ →	k_6

The reaction of O_2 with a radical P• is very fast and the reaction of hydrogen abstraction comparatively slow: typically $k_2/k_3 \gg 10^6$. We can thus imagine the existence of at least two kinetic regimes:

(i) The O_2 concentration is sufficiently high and all the radicals P• are almost instantaneously transformed into $PO_2^•$ ones. The termination processes (Equations 4 and 5) involving P• radicals can be neglected.

(ii) The O_2 concentration is lower than a critical value. A part of the radicals P• cannot then react with O_2 and will participate in other reactions, especially termination processes (Equations 4 and 5). We are obviously in conditions of diffusion-controlled kinetics.

Assuming that $k_5^2 = k_4 k_6$, one can obtain for the above scheme in the stationary state

$$-\frac{d[O_2]}{dt} = \frac{d[POOH]}{dt} = \frac{k_3 k_2 (r_i/k_4)^{1/2}[O_2][PH]}{k_2(k_6/k_4)^{1/2}[O_2] + k_3[PH] + (r_i k_6)^{1/2}} \quad (6)$$

Here $(r_i k_6)^{1/2} \ll k_3[PH]$, so that

$$-\frac{d[O_2]}{dt} \simeq \frac{k_2(r_i/k_4)^{1/2}[O_2]}{(k_2/k_3[PH])(k_6/k_4)^{1/2}[O_2] + 1} \quad (7)$$

Thus, for high oxygen concentrations

$$-\frac{d[O_2]}{dt} \simeq k_3(r_i/k_6)^{1/2}[PH] \quad (8)$$

and for low oxygen concentrations

$$-\frac{d[O_2]}{dt} \simeq k_2(r_i/k_4)^{1/2}[O_2] \quad (9)$$

In the case of radiation ageing (ionizing or ultraviolet radiation), it can be assumed that $r_i \simeq aI^{2\gamma}$ (a and γ are constants depending on the mechanism). This leads to

$$-\frac{d[O_2]}{dt} \simeq AI^{\gamma}$$

$$A = k_2 k_4 . [O_2] a^{1/2} \quad (10)$$

where γ is usually 0.5 or 1.0 depending on the chain mechanism (0.5 for the above mechanism).

2.1.3. The hyperbolic model of oxygen consumption

The above considerations lead to the conclusion that the oxygen consumption rate $r(C)$ is a hyperbolic function of the oxygen concentration C:

$$r(C) = \frac{\alpha C}{1 + \beta C}$$

$$\alpha = k_2\left(\frac{r_i}{k_4}\right)^{1/2} \quad (11)$$

$$\beta = \frac{k_2}{k_3[PH]}\left(\frac{k_6}{k_4}\right)^{1/2}$$

Two concentration domains can then be defined. For low values of C such that $\beta C \ll 1$, it can be considered that $r(C) \simeq \alpha C$. The system behaves as a first-order reaction. For high values of C such that $p_c \gg 1$, it can be considered that

$$r(C) \simeq \alpha/\beta \quad (12)$$

The system behaves as a zero-order reaction. Indeed, there is a "transition" domain, around $C_C = \beta^{-1}$, where the system will display an intermediate behaviour. In the case of LdPE irradiation, for a dose rate of 0.69 Gy s^{-1}, it was found that

$$r = \frac{ap}{1 + bp}$$

(p being the oxygen partial pressure), with $a = 5.57 \times 10^4$ cm^{-1} kGy^{-1} Pa^{-1} and $b = 3.6\,10^{-3}$ Pa^{-1} for LdPE. In other words, it can be considered that at atmospheric pressure, $r \simeq a/b$ and the system behaves as a zero-order reaction.

2.2. Oxygen profiles

The oxygen concentration profile can be determined from Equation 3:

$$D\frac{\partial^2 C}{\partial x^2} - r(C) = 0$$

This equation can be resolved with the following boundary conditions:

$$\left.\begin{array}{l} x = 0,\ t = 0 \\ x = L,\ t = 0 \end{array}\right\} C = C_s = pS^{-1}$$

(equilibrium oxygen concentration)

The local conversion in the thick sample will be

$$Q_{(x)} = \int_0^t r(C)\,dt \quad (13)$$

and the average conversion for the whole sample

$$\bar{Q} = \frac{1}{L}\int_0^L Q_{(x)}\,dx \quad (14)$$

Let us now consider the cases of first- and zero-order kinetics.

2.2.1. First-order kinetics

We can write

$$D\frac{\partial^2 C}{\partial x^2} - kC = 0 \quad (15)$$

where k is the first-order rate constant. This leads to

$$\frac{Q}{Q_S} = \frac{\mathrm{ch}\{\Phi[x - (L/2)]\}}{\mathrm{ch}[\Phi(L/2)]} \quad (16)$$

where

$$\Phi = \left(\frac{k}{D}\right)^{1/2} \quad (17)$$

The computed depth profile of Q/Q_s (relative or reduced conversion) is shown in Fig. 6. The thickness of the oxidized layer (TOL) is an increasing function of Φ^{-1}. In fact, it could be written

$$\mathrm{TOL} \simeq \Phi^{-1} = \left(\frac{D}{k}\right)^{1/2} \quad (18)$$

2.2.2. Zero-order kinetics above a critical concentration C_c

We can write

$$D\frac{\partial^2 C}{\partial x^2} - r_0 = 0 \quad (19)$$

With the same boundary conditions as above, this leads to

$$C = C_s + \frac{r_0}{2D}x(x - L) \quad (20)$$

where C_s is the equilibrium concentration. The concentration in the middle of the sample ($x = L/2$) is

$$C = C_s - \frac{r_0 L^2}{8D} \quad (21)$$

Here, the TOL could be assimilated to the half-thickness of a sample for which the concentration

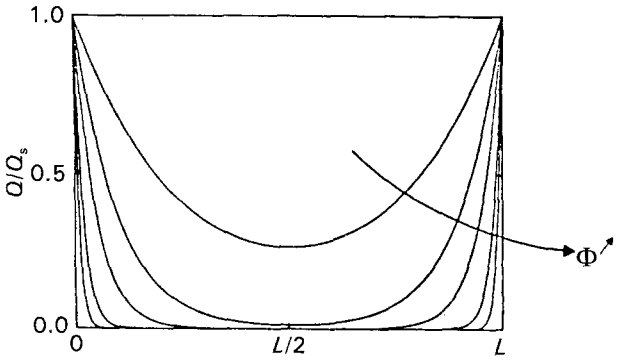

Figure 6 Computed shape of the reduced conversion for various values of Φ.

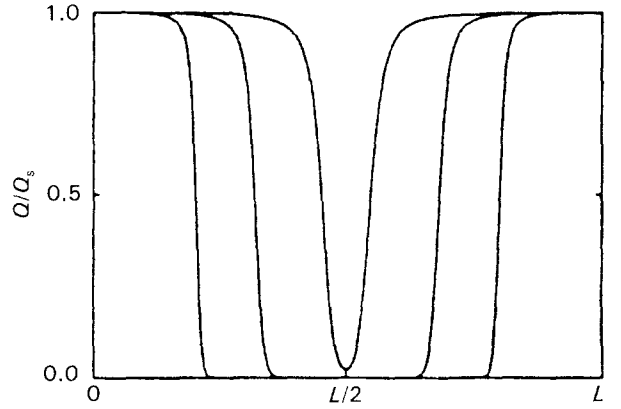

Figure 7 Computed shape of the reduced conversion for various values of Φ. TOL would be the length of the horizontal plateau.

reaches its critical value in the middle of the sample:

$$C_c = C_s - \frac{r_0(2\,\mathrm{TOL})^2}{8D}$$

$$\mathrm{TOL} = \left(\frac{2D(C_s - C_c)}{r_0}\right)^{1/2} \tag{22}$$

If we write $2(C_s - C_c) = \nu^2 C_s$, two simpler expressions for the TOL can be derived:

$$\mathrm{TOL} = \nu\left(\frac{Pp}{r_0}\right)^{1/2} \tag{23}$$

where $P = DS$ is the polymer permeability and p the oxygen pressure, and

$$\mathrm{TOL} = \nu\left(\frac{D}{k}\right)^{1/2} = \nu\Phi^{-1} \tag{24}$$

Here $r_0 = kC_s$ where $k = r_0/C_s$ is a pseudo-first-order rate constant varying with C_s; ν is a constant varying between 0 and $2^{1/2}$ when C varies between C_s and 0. The shape of depth distributions of the reduced conversion is shown in Fig. 7.

2.3. Conclusions

A first conclusion is that the thickness distribution of oxidation products can be computed if the oxygen diffusivity D and the expression of rate of oxygen consumption $r(C)$ against concentration C are known. In the general case, the basic differential Equation 2 can be numerically integrated. In two extreme cases, namely first-order and zero-order cases, this equation can be analytically resolved, which demonstrates the importance of the expression

$$\Phi^{-1} = \left(\frac{D}{k}\right)^{1/2} \tag{25}$$

where D ($m^2\,s^{-1}$) is the oxygen diffusion coefficient in the material and k (s^{-1}) is a pseudo-first-order rate constant determined by dividing the oxidation rate r_s in the superficial layer ($mol\,m^{-3}\,s^{-1}$) by the equilibrium oxygen concentration C_S ($mol\,m^{-3}$).

Φ^{-1}, which has the dimensions of length, is of the order of magnitude of the thickness of the oxidized layer (TOL). For the first-order kinetics

$$\mathrm{TOL} \simeq \Phi^{-1} \tag{26}$$

and for the zero-order kinetics

$$\mathrm{TOL} \simeq \nu\Phi^{-1}$$

$$\nu = \left[2\left(1 - \frac{C_c}{C_s}\right)\right]^{1/2} \tag{27}$$

C_c being the critical concentration above which zero-order kinetics can be applied.

A second conclusion is that L/Φ^{-1} can be used as a Deborah number. If the sample thickness L is such that $L/\Phi^{-1} < 1$, the oxidation is expected to occur homogeneously in the whole sample thickness. In contrast, if $L/\Phi^{-1} > 1$, the oxidation will be heterogeneous and the thickness of the oxidized layer would be of the order of magnitude of Φ^{-1}, except if C_c is of the order of magnitude of C_s. In this case $\mathrm{TOL} < \Phi^{-1}$.

3. Experimental methods

3.1. Whole kinetics

From measurements of the average conversion Q (Equation 14) it is possible to detect the boundary between no diffusion (I) and diffusion (II) controlled domains (Fig. 1). An example is given in the case of LdPE photo-oxidation [16], where the quantum yield for carbonyl formation was plotted against light intensity (for fluorescent lamps at $\lambda > 300$ nm) (Fig. 8). The quantum yield can be considered constant for intensities lower than 0.8×10^{19} photons $cm^{-2}\,h^{-1}$. The oxidation is not diffusion-controlled. For higher intensities, the quantum yield decreases with the intensity.

Another example is given in the case of the radiochemical ageing of plasticized PVC for which Gillen and Clough [17] studied the decrease of rupture elongation ε against dose, and determined the half-life dose $D(1/2)$ (dose to reduce ε for half of its initial value). Although a mechanistic cause was invoked by these authors for the observed dependency of $D(1/2)$ on the dose rate, it seemed interesting to us to plot $D(1/2)$ against the square root of the dose rate (Fig. 9). The existence of an almost linear dependence seems to be consistent with the above model for diffusion-controlled kinetics, provided that r_0 (or k) is proportional to the dose rate.

Many other examples of diffusion-controlled radiochemical ageing processes have been reviewed by

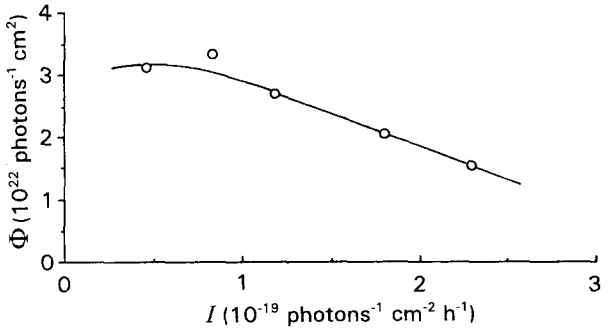

Figure 8 Quantum yield Φ of carbonyl formation against light intensity I for LdPE of 0.6 mm thickness irradiated in the near u.v. at 35°C, in air [16].

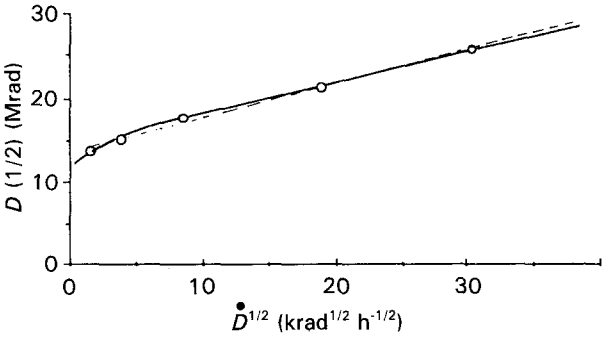

Figure 9 Radiochemical ageing of plasticized PVC from tensile ultimate property measurements. Half-life against square root of dose rate (adapted from results published by Gillen and Clough [17]; 1 rad = 10^{-2} Gy).

Wilski [18]. All the available experimental methods for ageing characterization can be used to determine apparent quantum yields, radiochemical yields or lifetimes.

3.2. Local kinetics

3.2.1. Measurements on microtome sections

Layers of 5 to 50 μm thickness can be cut using a microtome, at least in the case of unreinforced thermoplastics and thermosets. Reinforced plastics are difficult to machine if the filler size is of the order of or superior to the magnitude of the layer thickness. Rubber and semicrystalline samples with a T_g far below room temperature must be cooled.

Practically all types of physical and chemical determinations can be made on microtomed sections: u.v. and i.r. spectrophotometry, density measurements, viscosimetry in solution, etc. In the case of careful microtome sectioning, mechanical (tensile) testing can be performed on the individual layers [19].

Obtention of the first (superficial) layer is generally difficult for obvious reasons of sample roughness, sample curvature and geometrical positioning of the blade relative to the sample surface.

3.2.2. The microprobe approach

The analyses are made on a single transverse cut.

(i) Fluorescence microscopy was used many years ago by Ryan *et al.* [20] to study morphological effects on the spatial distribution of u.v. stabilizer. It can also be used to study the depth gradients linked to the kinetics controlled by diffusion.

(ii) A Raman microprobe can be used, although its efficiency is often severely limited by the sample fluorescence.

(iii) The i.r. microprobe is now practically a routine tool, more and more used in ageing studies [21].

(iv) Microhardness-like measurements have been used to establish modulus thickness profiles [10]. They are especially interesting for rubbers when noticeable changes of the crosslink density result from ageing.

(v) Changes of the refraction index can be monitored in glasses.

3.2.3. Use of experimental results

The above-mentioned methods have a spatial resolution whose order of magnitude is about 10 μm. According to the published data on this topic, the order of magnitude of the TOL during accelerated ageing is about 100 μm or higher, so that these methods can be used to establish the thickness distribution of degradation products.

In the case of a very fast initiation process, for instance oxidation during irradiation at dose rates higher than 100 Gy s^{-1}, plasma treatments, etc, the expected value of TOL is 1 μm or lower, and the above methods are obviously unsuitable. Electron microscopy, electron spectroscopy for chemical analysis (ESCA) and related methods can then be used.

In its domain of validity, a given method furnishes the following data:

(i) Q_s: conversion in the superficial layer.

(ii) $Q/Q_s = f(x)$: shape of the thickness distribution of reaction products.

(iii) TOL: thickness of the oxidized layer determined from $f(x)$ using an arbitrary criterion.

The variations of Q_s with time and exposure variables (temperature, intensity, etc.) allow one to establish the unperturbed (non-diffusion-controlled) ageing kinetics. The shape of $Q/Q_s = f(x)$ can also give an indication of the apparent kinetic order of oxygen consumption (see Figs 7 and 8). The variations of TOL with time and exposure variables are especially interesting in order to predict the material's long-term behaviour.

4. Examples of thickness profiles of reaction products

4.1. Radiochemical ageing of LdPE

Morphologically uniform measurements, unperturbed by processing, can be made on multilayer samples in which each elemental layer is a blown extruded LdPE film of 22 μm thickness. Multilayer samples are obtained by pressing together several films at 40°C, 0.2 MPa for about 20 min. It is then possible to separate the individual films after irradiation and to record their i.r. spectrum.

The thickness distribution of oxidation products can thus be obtained in a non-destructive way, and no

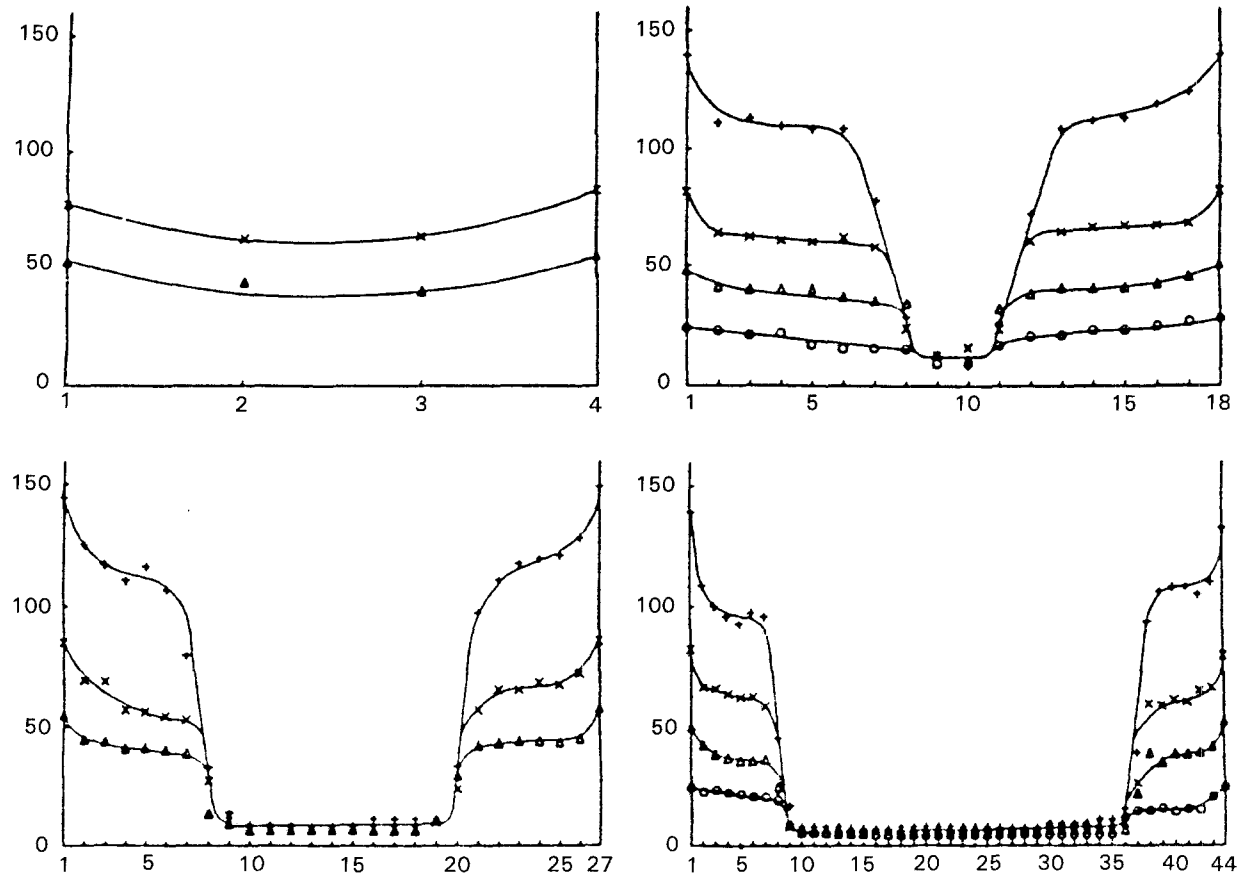

Figure 10 Depth distribution of carbonyl groups (carbonyl index) in irradiated (0.69 Gy s^{-1}) multilayer samples composed of 4, 18, 27, and 44 films of 22 μm thickness: (○) 0.14; (△) 0.30; (×) 0.45 and (+) 0.60 MGy [8].

disturbances can occur which are due to the skin–core structure induced in bulk samples by processing. The results obtained [8] on samples of various thicknesses at various doses of γ-rays in air, are presented in Fig. 10. It appears clearly that in the case under study:

(i) The TOL corresponds to about eight individual layers (≃181 μm) for the dose rate under consideration (0.69 Gy s^{-1}).

(ii) This TOL is independent of the whole sample thickness (as predicted by the model) and of the ageing time (or dose), which is due to the rate constancy with time (Fig. 4).

(iii) The thickness distribution displays a plateau corresponding to zero-order kinetics. As a matter of fact, the atmospheric pressure is noticeably higher than the critical pressure for a change of kinetic regime (Fig. 5).

(iv) Measurements made at 0.1 MPa oxygen pressure, i.e. about five times higher than atmospheric pressure, lead to a TOL of about 20 layers (against eight, for the same dose rate, at atmospheric pressure). The model predicts that

$$\frac{TOL_1}{TOL_2} = \left(\frac{p_1}{p_2}\right)^{1/2}$$

In the case under study:

$$\frac{TOL_1}{TOL_2} \simeq 2.50 \qquad \left(\frac{p_1}{p_2}\right)^{1/2} \simeq 2.24$$

The model can thus be considered valid within experimental scatter.

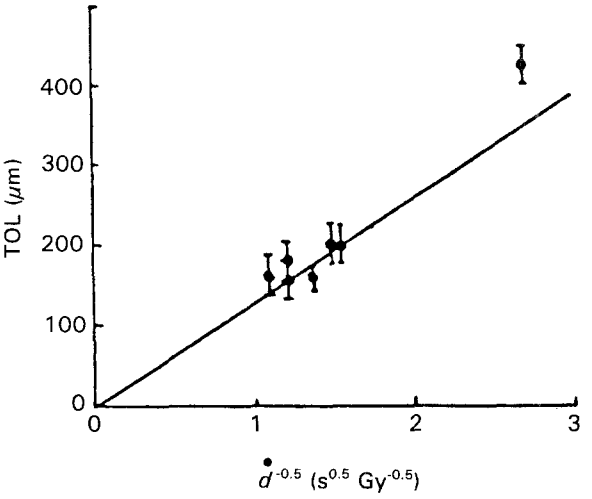

Figure 11 Radiochemical oxidation of LdPE. TOL against reciprocal of the square root of dose rate.

(v) For experiments made at various dose rates, the TOL was found almost proportional to the reciprocal of the square root of dose rate (Fig. 11). This is expected for a process in which the unperturbed rate r_0 would be proportional to the dose rate, or in other words the radiochemical yield $G(O_2)$ would be independent of the dose rate.

4.2. Thermal ageing of crosslinked polyethylene

Radiation-cured ribbons of XPE of 2.2 mm thickness were submitted to thermal ageing at temperatures

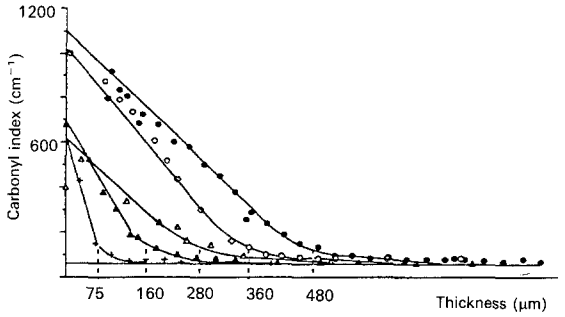

Figure 12 Thickness distribution of CO groups after (●) 1482 h at 130°C, (○) 354 h at 150°C, (▲) 66 h at 170°C, (△) 120 h at 160°C, (+) 23 h at 180°C.

ranging from 130 to 180°C [22]. The carbonyl groups were determined by i.r. spectrophotometry in microtomed sections. The oxidation in the superficial zone displays an induction time, as expected for stabilized PE in these exposure conditions. Some thickness distribution profiles of carbonyl group concentrations taken just after the induction period are shown in Fig. 12.

It appears clearly that, at least above the PE melting point (130°C for the sample under study), the TOL is a decreasing function of the temperature. This is not very surprising if we consider the basic relationship of Equation 18. If the diffusion process and the oxidation rate obey the Arrhenius law in the temperature interval under study, this can be written

$$\mathrm{TOL} = \left(\frac{D_0 \exp(-E_D/RT)}{k_0 \exp(-E_R/RT)}\right)^{1/2} = (\mathrm{TOL})_0 \exp\left(\frac{E_T}{RT}\right) \quad (28)$$

where

$$\mathrm{TOL}_0 = \left(\frac{D_0}{k_0}\right)^{1/2} \qquad E_T = \frac{E_R - E_D}{2}$$

In most of the thermal oxidation processes, $E_R > E_D \rightarrow E_T > 0$ and the TOL is a decreasing function of temperature as experimentally observed.

This is not necessarily true in the case of radio- and photo-oxidations where initiation (and branching), which play an important role in E_R for thermal ageing, have an activation energy of practically zero.

Another interesting consequence of Equations 18 or 24 is illustrated by Fig. 13, which shows the shape of the thickness distribution of the phenolic antioxidant both before and after the end of the induction period. In this figure it can be seen that the antioxidant is partially consumed during the induction period, and that its consumption is homogeneous. This is not surprising since, according to the model, if the oxidation rate is 100 times lower during than after the induction period, the TOL must be $100^{1/2} = 10$ times higher. Indeed, if the TOL is higher than the sample thickness, the distribution of oxidation products must appear homogeneous, as experimentally observed.

Just after the induction period, the sharp increase of the oxidation rate leads to the concentration profile

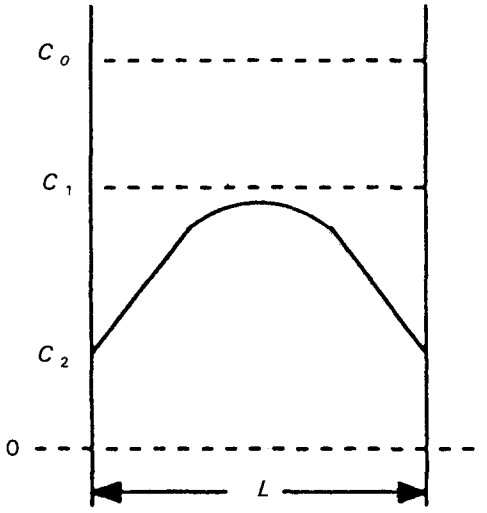

Figure 13 Shape of the thickness distribution of phenolic antioxidant, determined by u.v. spectrophotometry on microtomed sections: C_0 = initial concentration, C_1 = concentration just before the end of the induction period, C_2 = concentration just after the end of the induction period.

schematized by C_2 in Fig. 13. This result may be generalized as follows:

$$\left(\frac{D}{k(\mathrm{stab})}\right)^{1/2} \gg \left(\frac{D}{k(\mathrm{unstab})}\right)^{1/2}$$

Thus TOL(stab) ≫ TOL(unstab) because k(stab) ≪ k(unstab). In the case where the stabilization mechanism involves the consumption of stabilizer (by oxidation), this process is expected to be homogeneous over large thicknesses (compared to TOL in unstabilized samples in the same exposure conditions).

At the end of the induction period, the rate of consumption is increased in the superficial zone and a stabilizer concentration gradient appears, but the normal stabilizer diffusion tends to rehomogenize its distribution. It can be supposed that, if D(stab) is the stabilizer diffusion coefficient in the matrix, this tendency is expressed by the ratio $[D(\mathrm{stab})/k(\mathrm{consump})]^{1/2}$.

5. Problems of lifetime prediction in diffusion-controlled ageing

5.1. Basic principles of accelerated ageing

An experiment in accelerated ageing must be considered valid under the following conditions:

(a) The mechanisms responsible for property changes are the same as in natural ageing.

(b) An "aged state" can be defined from analytical measurements. A given "aged state" reached during natural ageing must be exactly reproduced during accelerated ageing.

In past years, attention was essentially paid to condition (a), i.e. essentially to the qualitative aspects of accelerated ageing. Using spectrometric, chromatographic, chemical methods etc. it is possible to show that both accelerated and natural ageing result in the formation of the same reaction products, eventually in the same ratio.

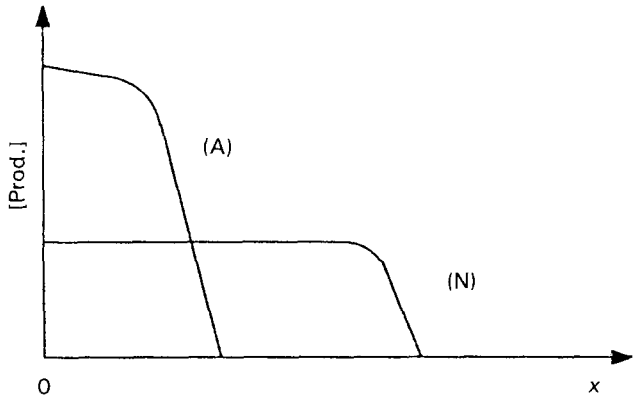

Figure 14 Schematization of the difference between degradation product distributions in the case of (N) natural ageing and (A) accelerated ageing resulting from an intensity increase, for a given average conversion.

Condition (b), in contrast, received considerably less attention despite its practical interest. As a matter of fact, the thickness of the degraded layer is of crucial importance in determining the residual mechanical properties of aged samples, as will be seen below. Some important consequences can be derived from the proposed model (Equation 25).

5.2. Aged state versus diffusion control

In the case of exposure to u.v. or ionizing radiations at a given temperature (close to the ambient temperature), the rate constant k is an increasing function of the radiation intensity, so that the TOL must decrease with the latter. Since, generally, the accelerated ageing is based on an increase of the intensity, the difference between "aged states" resulting from accelerated and natural ageing is as schematized by Fig. 14.

As will be seen below, the mechanical strength is a decreasing function of the thickness of the degraded layer (TOL in oxidation), so that for a given constant average conversion ratio of the degradation reaction, the effect on mechanical properties will be a decreasing function of radiation intensity. In other words, the "radiation yield" determined from a mechanical criterion will decrease with the intensity and therefore increase with the exposure time, for a given radiation dose.

5.3. Day–night alternation in photo-ageing

Two cases are to be considered.

5.3.1. Rectangular intensity signals

This is the case in many accelerated schedules, as schematized in Fig. 15. The resulting change of TOL is shown in the same figure. Indeed, the oxygen concentration increases during each dark half-period. The oxygen diffusion into a sample of thickness L can be represented by a characteristic time Z:

$$Z = L^2/D \qquad (29)$$

The order of magnitude of the oxygen diffusion coefficient at ambient temperature is 10^{-7}–10^{-5} $cm^2\,s^{-1}$ for a rubber and 10^{-8}–10^{-7} $cm^2\,s^{-1}$ for a glass. Thus, for a sample of 1 mm thickness, the order of magniude of Z would be 10^5–10^3 s for a rubber and 10^6–10^5 s for a glass.

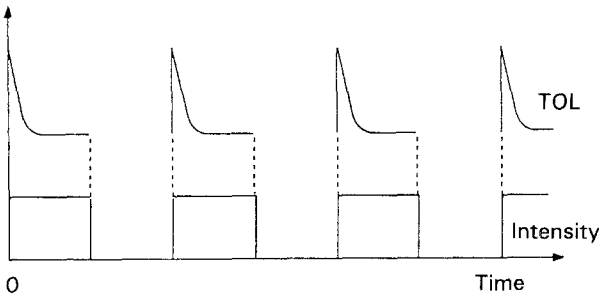

Figure 15 Expected profile of oxidation products during cyclic exposure.

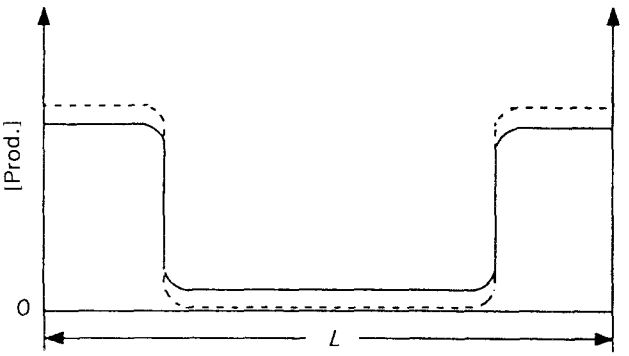

Figure 16 Schematic distribution of oxidation products: (—) during cyclic exposure, (– – –) during continuous exposure with the same dose. In the case of cyclic exposure there is a slight oxidation in the sample core, due to reoxygenation during the dark period.

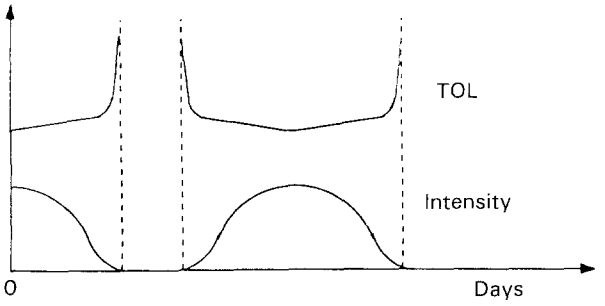

Figure 17 Changes of TOL during natural exposure, as expected from the model.

The light-off period is generally lower in the most widely used accelerated ageing schedules (for instance 102 min light, 18 min dark). The resulting distribution profile of oxidation products is schematized in Fig. 16.

5.3.2. Daily variations of the solar light intensity

In the case of an isothermal exposure, the changes of TOL would be as schematized by Fig. 17. In fact, the sample temperature T varies more or less in the same way as the light intensity, so that the variations of the diffusion coefficient with T must reduce the amplitude of TOL variations.

The duration of the dark period ($\sim 3 \times 10^4$ s) is of the order of magnitude of Z for rubber samples of

1 mm thickness. It remains lower for glassy materials of the same thickness (and for rubbers of higher thicknesses). It is easy to show that in the domain where the duration of the dark period is of the order of magnitude of Z, small fluctuations of exposure conditions can induce a considerable data scatter.

5.4. Accelerated ageing above a transition temperature

Accelerated thermal ageing is often made above the glass transition temperature T_g for glassy polymers or above the melting point T_m for semi-crystalline polymers. In these cases, the extrapolation of results to lower temperatures is highly questionable. As a matter of fact, a discontinuity is expected in the temperature variation of the diffusion coefficient. According to van Krevelen [44], the Arrhenius pre-exponential factor D_0 of the diffusion coefficient varies as follows:

$$\begin{aligned} T > T_m \quad & D_{01} \\ T < T_m \quad & D_{01}(1 - x_c) \\ T > T_g \quad & D_{02} \\ T < T_g \quad & D_{02}/10 \end{aligned}$$

where x_c is the crystalline fraction.

Indeed, the reaction rate can also undergo a discontinuity at these transitions, especially if the rate-determining step of the process is governed by the macromolecular mobility. It must, however, be supposed that the constancy (or the continuity) of the ratio D/k results only from a coincidence. Thus, the TOL variation with temperature is also expected to undergo a discontinuity around the glass transition or melting temperature, and this discontinuity must be taken into account in lifetime prediction models.

6. Consequences for mechanical behaviour

6.1. Basic structure–property relationships

A change of mechanical properties during long-term exposure can be due to various processes such as

(i) physical ageing (volume relaxation),
(ii) solvent absorption (plasticization swelling),
(iii) crystallization, orientation or stress relaxation,
(iv) cross-linking, chain scission.

In the general case of oxidative or hydrolytic ageing, the main cause of change of mechanical properties is the chain scission process. This section is essentially devoted to a study of the consequences of ageing dominated by chain scission.

Some physical and chemical aspects of these processes are well known. It will only be recalled that the conversion of a chain scission reaction can be expressed in terms of the number of scission events per gram of material, n_t (at time t). For a linear polymer, neglecting in a first approximation the polydispersity effects,

$$n_t = \frac{1}{\overline{M_{nt}}} - \frac{1}{\overline{M_{n0}}} \tag{30}$$

For a cross-linked polymer (at relatively low conversions)

$$n_t = \frac{1}{\overline{M_{c0}}} - \frac{1}{\overline{M_{ct}}} \tag{31}$$

where $\overline{M_{nt}}$ and $\overline{M_{n0}}$ are the values of the number-average molecular weight at time t and before exposure, respectively. $\overline{M_{ct}}$ and $\overline{M_{c0}}$ are the corresponding values of the average molecular weight of the elasticity active network segments.

Let us consider the case where the chain scissions are uniformly distributed in the whole sample volume. The sample can be compared to a virgin sample with the same average molar weight (and molar weight distribution). The available relationships between mechanical properties and molecular weight can then be used to predict the ageing-induced changes.

6.1.1. Linear polymers

The relationships between molecular weight and a given mechanical property cannot be in general represented by a single relation, and many cases are to be distinguished.

6.1.1.1. Initially brittle polymers. For very brittle materials, displaying a quasi-elastic behaviour until rupture, it may be considered that the strength is essentially linked to the cohesive energy density (CED). The ideal maximum stress σ_M would be given, according to Gardon [23, 24], by

$$\sigma_M = 0.25\,\delta^2 \tag{32}$$

δ being Hildenbrand's solubility parameter, where CED $= \delta^2$. If, according to this relationship, the strength is controlled by the structure at the molecular level (monomer unit), chain scission is expected to have very little influence except at very high conversions. Thus, in these conditions, the ultimate stress must vary very slowly with the degree of degradation, which is experimentally observed.

In polymers such as poly(methyl methacrylate) (PMMA) or polystyrene (PS), which can be considered brittle under normal tensile conditions, fracture mechanics allows one to demonstrate molecular weight effects. An interesting criterion here is G_c, the critical

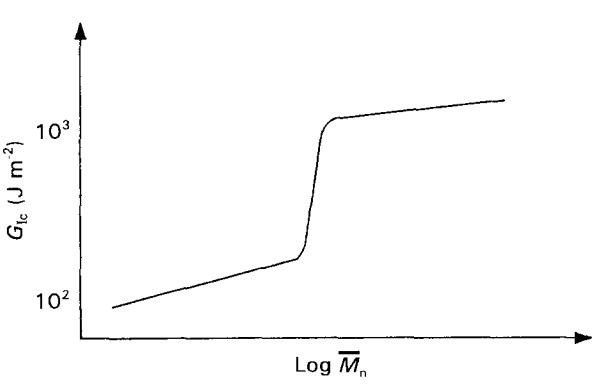

Figure 18 Shape of G_{Ic} variations with the logarithm of molecular weight for linear polymers.

energy for surface formation (rate of elastic energy release). When it is plotted against $\overline{M_n}$, it reveals a relatively sharp transition [25] (Fig. 18).

For low values of $\overline{M_n}$, the polymer is very brittle ($G_c \leqslant 100\,J\,m^{-2}$). Above a critical value of $\overline{M_n}$, often about $10^4\,g\,mol^{-1}$, the polymer is relatively tough ($G_c \geqslant 1000\,J\,m^{-2}$), and the transition between both regimes of cracks propagation kinetics is relatively sharp (in a logarithmic molecular weight scale). Above this transition, G_c tends to become practically independent of $\overline{M_n}$.

6.1.1.2. Initially ductile thermoplastic polymers. For glassy or semi-crystalline polymers exhibiting ductile behaviour, random chain-scission ageing can be generally described as a ductile–brittle transition. In a tensile test, it has been observed that the ultimate elongation varies as shown in Fig. 19.

The ultimate elongation remains first almost constant (except for crystallization or plasticizer migration processes), decreases quickly after a critical ageing time t_c, and then reaches a plateau value corresponding to the original yield strain ε_y. The same behaviour can be observed for the impact strength (Fig. 20).

It is noteworthy that, in these cases, modulus variations are generally neglectable, and that the rupture envelope (ultimate stress versus ultimate elongation) is generally the initial tensile curve. This is valid as well in the photochemical ageing of linear polymers [26] as in the hydrolysis of polycarbonate [27].

It is generally recognized that the ductile–brittle transition, as shown in Figs 19 and 20, is associated with a critical value M_c of the molecular weight. For $M > M_c$, the chains are entangled and the entanglements behave as physical cross-links, allowing large-scale deformations of the network segments. In the case of semi-crystalline polymers, the concentration of tie molecules (molecules which interconnect the crystallites) increases also with the fraction of chains of molecular weight much higher than M_c. For $M < M_c$, the polymer strength is essentially governed by the intermolecular interactions (van der Waals forces), which corresponds to rupture energies one order of magnitude lower than in the case of segment orientation. Thus, according to these theories, embrittlement would occur in a homogeneous sample when the molecular weight reaches M_c. This seems to be verified in the case of the non-diffusion-controlled hydrolysis of polycarbonate (PC), for which the ductile–brittle transition occurred at $M_c \simeq 34 \times 10^3\,g\,mol^{-1}$. This value is probably somewhat higher than the entanglement limit but by less than one order of magnitude.

The existence of a critical molar weight M_c allows us to define a critical number of chain scissions per mass unit n_c:

$$n_c = \frac{1}{M_c} - \frac{1}{\overline{M_{n0}}} \tag{33}$$

The chemical kinetics allows us to establish the relation between the reaction rate and the time and exposure variables:

$$n_t = f(t) \tag{34}$$

which in turn allows us to define a lifetime t_c:

$$t_c = f^{-1}(n_c) \tag{35}$$

where f^{-1} is the reciprocal function of $f(t)$. t_c is the time after which an initially ductile and/or tough sample becomes brittle as a result of a homogeneous random chain-scission ageing process.

6.1.2. Cross-linked polymers

The above features have also been observed in the case of thermosets, for instance during the thermal oxidation of epoxies [13, 14] or during the hydrolysis of

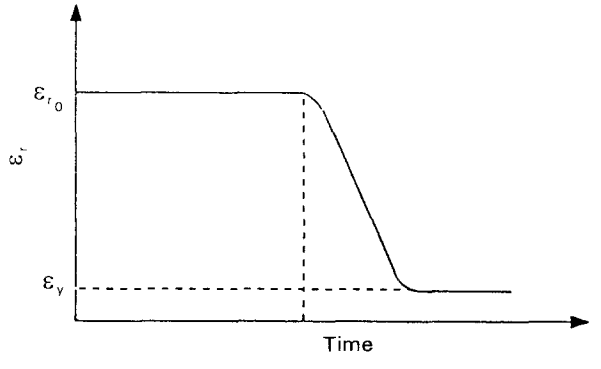

Figure 19 Shape of ultimate elongation variations for a random chain-scission ageing process.

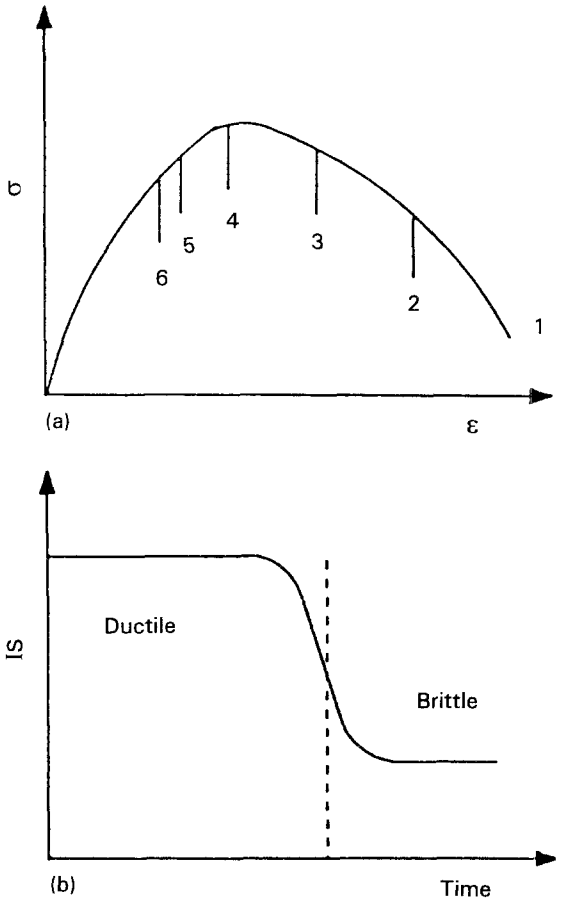

Figure 20 (a) Shape of the stress–elongation curves for impact tests on samples of ageing time increasing from 1 to 6. (b) Shape of the time change of impact strength showing the relatively sharp ductile–brittle transition.

polyesters [28]. In the case of rubbers, however, noticeable differences are to be expected. For instance, as a result of the rubber theory of elasticity, the modulus must decrease linearly with the chain scission conversion. For low conversions

$$G(t) = G(0) - \phi n_t \quad (36)$$

where $G(t)$ and $G(0)$ are the shear moduli after and before ageing and ϕ is a factor derived from rubber elasticity theory. The changes of ultimate stress and ultimate elongation can also be predicted from rubber elasticity theory or from empirical considerations [29].

6.2. Heterogeneous (skin–core) aged samples

In the case of a diffusion-controlled ageing process, it is well known that embrittlement depends essentially on the local (superficial) rather than the average degradation conversion. In other words, an embrittlement of the superficial layer can make the whole sample "sensitive" to rupture. Fracture mechanics models are in principle adequate to describe this situation. The aim of this section is to review the literature on this topic.

In 1968, Bucknall and Street [30] compared the effects of temperature, specimen geometry and polymer composition on the impact (bending) strength. They did this both for aged specimens of high-impact PS (HIPS) and acrylonitrile–butadiene–styrene (ABS) and unaged specimens of HIPS and ABS laminated with PS and styrene aerylonitrile (SAN), respectively. They suggested that u.v. degradation, and a notch or a layer of a brittle glassy polymer, reduces the energy of crack initiation. As a result the impact strength is mainly determined by the crack propagation energy.

The geometry of the specimen they used is shown in Fig. 21. The results for the brittle layer specimens are in good agreement with the results of u.v.-degraded samples. However, u.v. exposure tests remain necessary to determine whether surface embrittlement takes place, and to what extent.

In 1972, Ruhnke and Biritz [31] suggested that the bending stress causes a crack in the brittle layer which under specified conditions could easily propagate through the substrate. The impact behaviour of an aged ABS specimen could be compared to that of a composite consisting of a brittle coating with good adhesion to a ductile substrate.

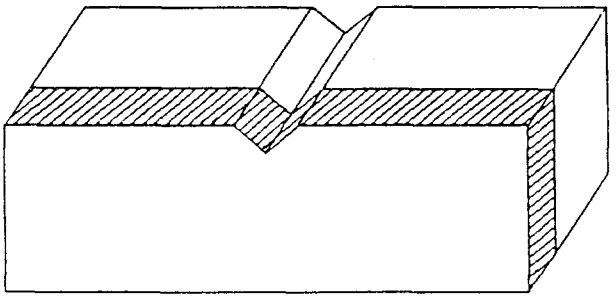

Figure 21 Brittle layer impact specimen used by Bucknall and Street [30] to simulate the effect of u.v. degradation on the failure behaviour.

In 1974, Priebe and Stabenow [32] stated that ABS has a sudden and steep decrease of the impact strength to the level of the notched impact strength. While this is normally explained in terms of a notch reaching a critical depth which initiates fracture, they suggest that this fracture mechanism does not correspond to that of a u.v.-degraded sample. After the samples were exposed outdoors for 10 days, they showed a strong decrease in impact energy. However, no cracks could be found in the degraded surface, even after 21 days when the impact energy had reached its end-level. The depth over which the material was affected was found by comparison of the contrast of different films cut from the degraded surface with the contrast of undegraded films, as seen by means of an optical microscope. The impact toughness strongly decreased at a certain critical depth of affected material.

They also tested duplex samples with SAN layers with different thicknesses on top of ABS. The thickness of the layer that caused a dramatic decrease of the impact energy was comparable to the depth of affected material found in the aged samples. They assumed a failure mechanism in which the stress in the (outer) brittle layer quickly reaches a high value in bending until a crack initiates and propagates. Unstable crack extension occurs as soon as the crack becomes larger than the critical crack length. This raises the velocity, so the crack will propagate at a high velocity through the substrate. It is assumed that the thickness of the layer has to be larger than a critical crack size, in this case 10–20 μm (note that this is very small).

In 1976, Carlsson and Wiles [33] reasoned that for polypropylene (PP) the lack of correlation between bulk oxidation, as measured by i.r. spectroscopy, and tensile failure, was caused by the fact that the oxidation could only occur in a surface layer (< 500 μm). They suggested that complete failure could occur when the sample is stressed after the spontaneous formation of cracks in the thin oxidized surface layer. They attributed this to the notch sensitivity of PP.

In 1981, Wolkowicz and Gaggar [34] found a critical thickness of the thermo-degraded surface layer for ABS, of 200 μm, which causes brittle failure of the entire sample. When they tested oven-aged samples it was shown that, after removal of the degraded surface layer, the ductility of the samples was restored.

In 1982, So and Broutman [35] studied surface embrittlement by laminating brittle polymer films, PS and SAN, on to HIPS and ABS to simulate both embrittlement due to environmental degradation and brittle paint systems. They studied the effect of varying coating thickness and molecular weight on the strength in tensile and impact testing. They concluded that the energy absorbing capability of rubber-toughened polymers is severely restricted, particularly when the coating thickness reaches a critical value at which a single surface crack is able to propagate across the coating–substrate interface in an unstable manner. In these cases it is suggested that the crack impinges on the coating–substrate interface at a high velocity, which effectively enhances the local strain rate at the crack tip. Therefore it is reasonable to expect a reduction of the substrate fracture toughness,

so that the rapidly moving crack can easily propagate through the substrate. Thus, the ultimate fracture strain of the coated sample coincides with that of the coating polymer. They suggested that the critical coating thickness is equal to the critical crack size just prior to the onset of unstable crack growth:

$$Y\sigma a_c^{1/2} \geqslant K_{Ic}(\text{ABS})$$

In 1982, Rolland *et al.* [36] presented a paper on a fracture mechanics approach to surface embrittlement in ductile polymers. In 1983, Rolland and Broutman [37] presented the same paper and added some theoretical considerations on shear stress and interfacial bonding, as well as results on experimental determination of the dynamic stress intensity factor. These results are a verification of their theory. Rolland *et al.* described the necessary conditions for one of the three modes which can occur if a crack (which is initiated in the brittle surface layer) arrives at the brittle–ductile interface. The crack can

(i) be arrested at the interface,
(ii) propagate across the interface and be arrested in the ductile material,
(iii) propagate completely through the sample.

The necessary condition for a crack to propagate completely through a sample is

$$[(K_{Id})_{\text{brittle}}]_{\text{interface}} > (K_{Id})_{\text{ductile}} \quad (37)$$

This means that, in order to get complete fracture, the crack velocity-dependent stress intensity (K_{Id}) in the brittle material should have reached a value at the interface which lies above the crack arrest value of the ductile material.

The critical velocity at the brittle–ductile interface for the duplex specimens was measured. The crack growth velocity ($\dot{a}$) versus dynamic stress intensity (K_{Id}) was measured for both ductile PC and brittle PMMA material. The result is given in Fig. 22. This shows that the critical crack velocity at the brittle–ductile interface (in this case 320 m s^{-1}) can be predicted from the $\dot{a}$ versus K graph for both the ductile and the brittle material.

In 1983, Rosenzweig and Broutman [38] presented a paper about the surface embrittlement of high-density polyethylene (hdPE). Their research was to determine the mechanical properties of a brittle surface layer formed by u.v. radiation and its influence on the failure behaviour of hdPE. This characterization is done on samples degraded for 720 h in an Atlas Intensive UVCON chamber at 45°C. They tried to compare the mechanical behaviour of u.v.-degraded tensile samples with that of razor-blade-notched samples.

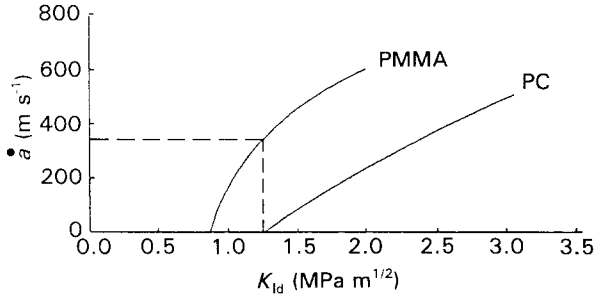

Figure 22 Relation between crack velocity ($\dot{a}$) and dynamic stress intensity (K_{Id}) for PMMA and PC [38].

They mentioned the role of u.v. exposure in generating a residual stress distribution, without going into details. They found that the crystallinity at the surface, measured by differential scanning calorimetry (DSC), was higher than that of the virgin material, possibly due to chemicrystallization. By cutting away the unaffected material, they found an increase in the tensile modulus of elasticity from about 690 MPa for a 6.35 mm thick sample to a very high value of 2930 MPa for a 180 μm thick sample. The thickness of the embrittled layer, measured with an optical microscope, was ~300 μm. By removing thin layers from the exposed surface, they found that when 150 μm was removed, the failure mode changed from brittle to ductile.

In razor-blade-notched samples they found that when the depth was more than 750 μm, the failure changed from ductile to brittle. They explained the discrepancy between aged and notched samples by suggesting that the brittle surface serves as a self-notching device. Notches are generated at a very low strain, probably not high enough to generate orientation and crack blunting to inhibit further crack propagation. Moreover, the degraded surface layer becomes highly stressed because of its high stiffness, thus providing the crack with an initially high potential energy.

In 1985, Rolland and Broutman [39] presented their work on the measurement of K_{Ic}, K_{Ia} and the $\dot{a}$ versus K curve. They concluded that the value of K_{Ia} is less dependent on specimen variables, temperature and strain rate than K_{Ic}.

In 1985, So and Broutman [40] used the J integral technique to determine the ductile fracture toughness for ABS and HIPS. From the measured J_{Ic} value they calculated the critical crack size, which determines the onset of rapid crack extension, for two ductile materials (ABS and HIPS) and two brittle materials (SAN and PS), according to

$$a_1 = \frac{J_{Ic}E}{4\sigma_f^2} \quad (38)$$

They found that the critical thickness of a brittle coating on a ductile substrate corresponds well to the critical crack size of the brittle coating. They suggest that when a crack depth a_1 is reached, the crack velocity increases drastically, followed by an increase in the K value (see Figs 23 and 24). Thus brittle fracture occurs because the K value of the brittle material at a high crack velocity becomes equal to the K_m value of the ductile substrate. Here, the subscript in K_m denotes the minimum fracture toughness of the substrate. It should be noted that the K_m value is the same as the K_{Ia} value used by Rolland and co-workers [35, 40, 41].

In 1986, Broutman and Rolland [41] presented their latest theory and results, following the papers on surface embrittlement of So and Rolland together with Broutman from 1982 to 1985 [38, 40]. The objective of their research was to investigate whether the theory of

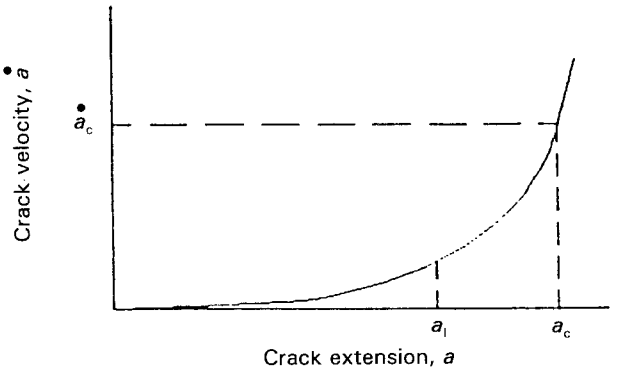

Figure 23 Crack velocity versus crack extension [40]: (a_1) = critical crack dimension for fast crack growth. a_c = critical crack dimension for brittle fracture.

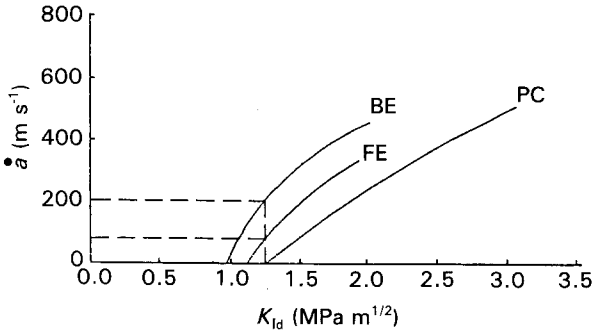

Figure 25 Effect of the dynamic stress intensity factor K_{Id} on the crack velocity for polycarbonate (PC), brittle epoxy (BE) and flexible epoxy (FE) [41].

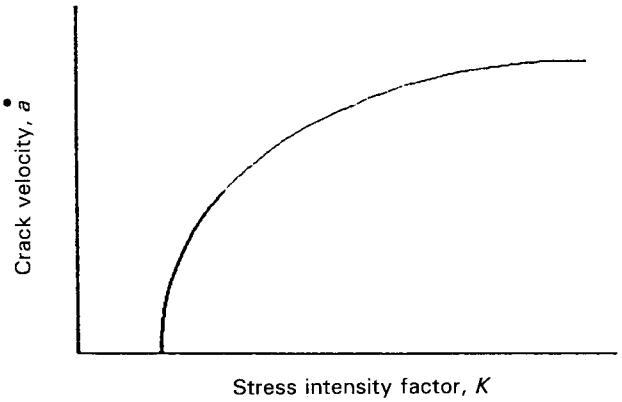

Figure 24 Suggested curve showing the dependence of crack velocity on the crack driving force [40].

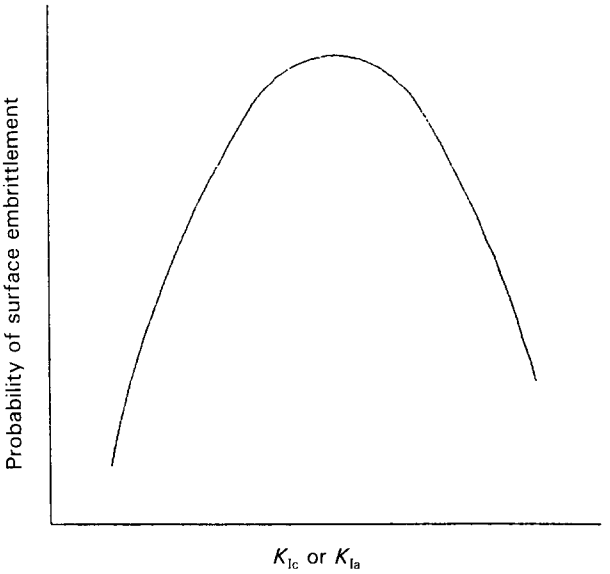

Figure 26 Schematic representation of the probability of surface embrittlement as a function of both the fracture toughness K_{Ic} and the crack arrest toughness K_{Ia} [41].

the critical crack velocity applies also to thin brittle surface layers. Brittle and more ductile epoxy layers were used as coatings on PC and ABS. A crack is initiated as soon as the brittle layer is stressed and the strain in the brittle layer exceeds its critical strain, independent of the coating thickness. The crack will penetrate the ductile surface if the coating thickness is larger than the critcal thickness. If the coating thickness is smaller than the critical thickness, the crack is arrested. Either delamination of the layer occurs (in the case of PC) or multiple cracks are formed in the brittle layer (in the case of ABS), due to the increasing elongation. In ABS, one crack will penetrate the ductile material due to strain-hardening of the ABS, which is believed to decrease the value of the crack arrest toughness.

Fig. 25 shows the agreement between the values of the critical velocity measured at the brittle–ductile interface (90 and 200 m s^{-1}) and the theory based on the separately measured $\dot{a}$ versus K curve. The critical coating thickness and crack velocity are lower for a ductile epoxy than for a brittle epoxy because the K_{Id} value of the ductile epoxy is larger than that of the brittle epoxy (for any crack velocity). Thus for the same coating thickness the flexible epoxy will give a higher crack velocity at the brittle–ductile interface.

Fig. 26 shows how the probability of surface embrittlement depends not only on K_{Ia}, but also on K_{Ic}. An extremely brittle coating does not release enough energy or possess a large enough value of K_{Id} to exceed the arrest toughness of the ductile substrate and will not induce embrittlement. Thus, to embrittle a material, K_{Ic} should not be too large to enable crack initiation. On the other hand it should not have a very low value of K_{Id}, in which case the crack would not have enough energy to propagate across the interface.

In 1988, Schoolenberg [42, 43] compared notched specimens with u.v.-degraded specimens in impact where the notch depth was equivalent to the depth of embrittlement, measured by means of (e.g.) i.r. spectroscopy. She concluded that the depth of embrittlement is not the only determining factor for a quantitative prediction of the fracture energy [43]. She found three stages of failure behaviour for degraded PP which could be compared to the fracture energy of a notched sample with an equivalent depth, as shown in Fig. 27. The stages mentioned in Fig. 27 occur under different circumstances and are tabulated in Table 1. The most important deviation of the failure behaviour of u.v.-degraded samples from that of notched samples was seen after relative short exposure times, (stage IIb). Schoolenberg explained the deviation by the so-called crack speed effect. A crack initiated in the embrittled layer will achieve a high velocity as it reaches the brittle–ductile interface and this will lower the fracture

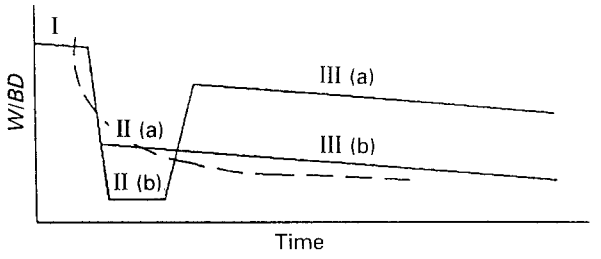

Figure 27 Three stages in fracture behaviour [42]: (I) initiation time, (IIa) moderately brittle behaviour, (IIb) very brittle behaviour, (IIIa, IIIb) stable end level; (– –) notched specimens.

TABLE I Occurrence of the stages mentioned in Fig. 27 dependent on material, processing method and test velocity [41]

Test velocity	Compression-moulded (non-stabilized and stabilized)	Injection-moulded	
		Non-stabilized	Stabilized
High	I–IIb–IIIb	I–IIb–IIIb	I–IIa–IIIa
Low	I–IIa–IIIa	I–IIb–IIIa	

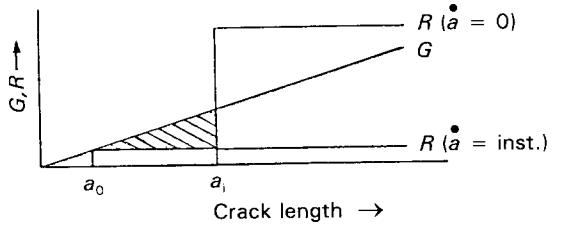

Figure 28 Crack speed effect caused by the decrease of the fracture resistance R when $\dot{a} > \dot{a}_{instability}$.

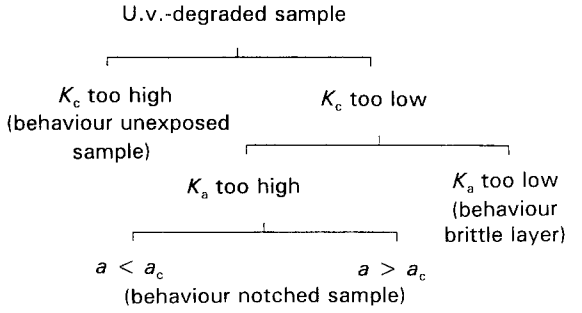

Figure 29 Possible modes of failure of a duplex sample.

toughness of the ductile material, so the crack can pass the interface unnoticed (Fig. 28). It was stated that the conditions for continuing crack propagation are given by $\dot{a} > \dot{a}_{instability}$ and Equation 38.

The different failure modes of an aged sample can thus be summarized by the scheme given in Fig. 29.

References

1. R. C. GOLIKE and S. W. LAZOSKI, *J. Phys. Chem.* **64** (1960) 895.
2. G. C. FURNEAUX, K. J. LEDDURY and A. DAVIS, *Polym. Degrad. Stab.* **3** (1986) 431.
3. A. V. CUNLIFFE and A. DAVIS, *ibid* **4** (1982) 17.
4. T. SEGUCHI, S. HASHIMUTO, K. AKAKAWA, N. HAYAKAWA, W. KAWAKAMI and J. KURYAMA, *Rdiat. Phys. Chem.* **17** (1981) 191.
5. S. P. FAIRGREVE and J. R. McCALLUM, *Polym. Degrad. Stab.* **11** (1985) 251.
6. J. R. PUIG, "*Les techniques de l'Ingéniew-Génie nucléaire*" (*Paris*) *B* **3770** (1982) 1.
7. M. V. BELUSOVA and V. D. SKIRDA, *Acta Polym.* **10** (1985) 36.
8. G. PAPET, L. AUDOUIN-JIRACKOVA and J. VERDU, *Radiat. Phys. Chem.* **33** (1989) 329.
9. S. G. KIRYUSHKIN and Y. A. SHLYAPNIKOV, *Polym. Degrad. Stab.* **23** (2) 185.
10. K. T. GILLEN and R. L. CLOUGH, in "Handbook of Polymer Science and Technology", Vol. 2, edited by N. P. Cheremisinoff (Dekker, New York, 1989) p. 170.
11. G. S. PARK and J. CRANK, "Diffusion in Polymers" (Academic, New York, 1981) pp. 4–20.
12. L. AUDOUIN and J. VERDU, *ACS Symp. Ser.* **475** (1991) 473.
13. M. LEHUY, thesis, ENSAM, Paris (1990).
14. *Idem, Polym. Degrad. Stab.* in press.
15. J. PETRUJ and J. MARCHAL, *ibid.* **16** (1980) 27.
16. A. HUVET, J. PHILIPPE and J. VERDU, *Euro. Polym. J.* **14** (1978) 709.
17. K. T. GILLEN and R. L. CLOUGH, *J. Polym. Sci., Polym. Chem. Edn.* **19** (1985) 2041.
18. H. WILSKI, *Radiat. Phys. Chem.* **29** (1) (1987) 1.
19. de J. C. M. BRUIJN, thesis, Delft University Press, 1992.
20. T. G. RYAN, P. D. CALVERT and N. C. BILLINGHAM, "Stabilization and Degradation of Polymers", ACS Chemistry Series Vol. 169 p. 261.
21. X. JOUAN and L. GARDETTE, *Polym. Commun.* **28** (1987) 239.
22. V. LANGLOIS, M. MEYER, L. AUDOUIN and J. VERDU, *Polym. Degrad. Stab.* **40** (1993) 399.
23. J. L. GARDON, *J. Coll. Interf. Sci* **59** (1977) 582.
24. *Idem, Progr. Org. Coatings* **5** (1977) 1.
25. H. H. KAUSCH, in "Interrelations between Processing, Structure and Properties of Polymeric materials", edited by J. C Seferis and P. S. Theocaris (Elsevier, Amsterdam, 1984) p. 363.
26. J. PABIOT and J. VERDU, *Polym. Eng. Sci.* **21** (1) (1981) 32.
27. R. J. GARDNER and J. R. MARTIN, *J. Appl. Polym. Sci.* **24** (1979) 1269.
28. B. MORTAIGNE, thesis, ENSAM, Paris (1989).
29. J. VERDU, B. MORTAIGNE and P. A. HOARAU, in Proceedings of 11th International Conference on Advances in the Stabilization and Controlled Degradation of Polymers, Luzern, 24–26 May 1989.
30. C. B. BUCKNALL and D. G. STREET, *J. Appl. Polym. Sci.* **12** (1968) 1311.
31. G. M. RUHNKE and L. F. BIRITZ, *Plast. Polym.* **6** (1972) 118.
32. E. PRIEBE and J. STABENOW, *Kunststoffe* **64** (1974) 497.
33. D. J. CARLSSON and D. WILES, *J. Macromol. Sci. C* **14** (1) (1976) 65.
34. M. D. WOLKOWICZ and S. K. GAGGAR, *Polym. Eng. Sci.* **21** (1981) 571.
35. P. SO and L. J. BROUTMAN, *ibid.* **22** (1982) 888.
36. L. ROLLAND, K. THOMSON, S. MOSTOVOY and L. J. BROUTMAN, in Proceedings of International Conference on Deformation, Yield and Fracture of Polymers, Cambridge, 1982.
37. L. ROLLAND and L. J. BROUTMAN, in Proceedings of ANTEC 83, May 1983 (1983) p. 451.
38. N. ROSENZWEIG and L. J. BROUTMAN, *ibid.* p. 455.
39. L. ROLLAND and L. J. BROUTMAN, in Proceedings of ANTEC 85 (1985) p. 634.
40. P. SO and L. J. BROUTMAN, *ibid.* p. 639.
41. L. J. BROUTMAN and L. ROLLAND, in Proceedings of ANTEC 86, April 1986 (1986) p. 600.
42. G. E. SCHOOLENBERG, thesis, Technical University of Delft (1988).
43. *Idem, J. Mater. Sci.* **23** (1988) 1580.
44. D. W. VAN KREVELEN and P. J. HOFTYZER in "Properties of Polymers" (Elsevier Scientific, New York 1976) p. 410.

Received 9 July
and accepted 30 July 1992